Modelling of Drying Tropical Fruits using Multiphase Model

N. SHAHARI
Universiti Teknologi MARA
Faculty of Computers and Mathematical Sciences
Negeri Sembilan Campus
MALAYSIA
norazni@ns.uitm.edu.my

S. HIBBERD
University of Nottingham
School of Mathematical Sciences
University Park, Nottingham
UNITED KINGDOM
stephen.hibberd@nottingham.ac.uk

Abstract: Single-phase heat and mass models have been widely used to describe the movement of moisture and heat during drying of food products. This model often taken food as a homogeneous medium and does not allow to incorporate more detailed ongoing processes inside the fruits tissues during drying. Hence, this paper focuses on the development of a model to describe the movement of moisture and heat during drying of fruits that is based on their cellular structure and model are derived using multi-phase approach. Specifically, mathematical model is developed to utilizing COMSOL Multiphysics to solve the equations governing the transport of moisture and heat in order to predict the moisture lost during drying of fruit. Simulation of multi-phase model yield result similar with single-phase model and also generates result not evident in homogeneous model such as water vapour in intercellular space. The results show that the moisture decreased due to the effect of the temperature, water vapour and bound water. However, bound water has no influence at the beginning of drying, while plays a significant role at the later stage of drying. Moreover, pressure plays a significant role on transport of liquid water from one cell to another cell which associates by plasmodesmata transport. The results obtained herein can provide some new theoretical guidelines for the development of drying model.

Key–Words: Drying, food, multiphase, heat, mass.

1 Introduction

In recent years, more comprehensive theories have been developed to describe the simultaneous heat and mass transfer processes on a microscopic scale, on the basis of diffusion theory, capillary flow theory, and evaporation condensation theory. In particular, increasing attention on heat and mass transfer in porous media has resulted in many experimental and theoretical investigations for different applications. For example, Luikov's equation and Whitaker's approach are usually used for non-hydroscopic material, such as sand, polymer particles and ceramics where the transport of material does not cause additional complications and the phases are clearly separated. For food material, which is hydroscopic porous media, an equivalent porosity and equivalent water saturation have been introduced by researchers such as [1, 2, 3, 4, 5, 6]

Perhaps the earliest model in food that included pressure driven flow was Farkas *et al.* [7]. A two region detailed model was developed - core and crust - providing different sets of equations for these two regions, separated by a moving boundary and showing differences in temperature between them. The physical assumption was made that liquid water flow took place within the core region and that water vapor movement was pressure-driven only in the crust region. Although Farkas' model was able to include the structure of the food, it failed to model or capture the interaction between the two-phase regions, only the moving boundary that separated the two-regions.

Ni and Datta [8] extend the model by Farkas by adding the oil phase conservation equation, with the introduction of equivalent porosity and equivalent water saturation. They added capillary flow in liquid water transport and diffusive flow in vapour transport, which are not considered in Farkas' model. They considered only one region with three-phases in continuum: the liquid phase combination of equation of water vapour and liquid water in term of one equation of the liquid phase, the air phase and the oil phase. The conservation equations for vapour, liquid water, air and energy are written and the conservation equation is transformed into variable saturation S_w, temperature T and pressure P as in the Luikov approach. However, further experiments investigation by Halder *et al.* [9], most water is not in the pores but in the cell, so the use of equivalent water saturation analogous to porous media is not appropriate. Thus, an improved model was suggested that would replace the instantaneous phase change of liquid water to vapour by in-

troducing an evaporation rate term equation and using non-equilibrium approach derive from an expression by Fang and Ward [10]. Since water vapour is not always in equilibrium with liquid water, Ousegui *et al.* [5] and Halder *et al.* [11], developed a multiphase model using a non-equilibrium formulation for evaporation, which is the latest mathematical modelling for drying and frying.

All the models discussed above developed a formulation analogous to those equations well-established for non-hygroscopic porous media but do not reflect the complexity of cellular structure in their modelling. Structure heterogeneity of biological material, such as fruit, brings additional complexity to the water migration in a porous solid system. An interesting study regarding cellular material is made by [12]. In this work, the author applied Whitaker's model to investigate the isothermal drying of cellular materials with the influence of shrinkage. It was shown that water transport during drying occurs by the contribution of three fluxes, and a very precise equation for the fluxes was developed. This will be more relevant than the development of a formulation analogous to those equations well-established for non-hygroscopic porous media. Following this mechanism, the present study focuses on movement of several phases, for example liquid phase and vapour phase: these will form the basic of multi phase model.

The objective of this paper is to investigates by means of mathematical modelling heat and mass transfer phenomena during drying of fruits by developing representative model based on theirs cellular structure. The basic two-phase transport of water vapour, as a mixture of air and water vapour through the pores is considered as flow through a porous structure, that interacts with the cell structure. The analysis of this paper uses mathematical modelling to investigate the effect of bound water, water vapour, internal turgor pressure on the distribution of moisture and temperature during drying.

2 Formulation

The theory of previous study of food drying is construct, starting from a realistic picture of cellular tissue. Cellular fruit tissues are taken as a combination of cell body, cell wall and membrane and intercellular space as shown in Fig 1 and as given by [13]. A representative cell of this type is like a cellulose capsule filled with liquid. Moisture in the drying of fruits is taken to exist in three categories: water vapour in the pores, free liquid water inside the individual cells and bound water held within the solid cell structures. In this case, liquid water can migrate out of the cell in three possible ways: transmembrane transport through tonoplast and plasmalemma membrane boundaries, sympalstic transport involving transport of water from one cell directly into another by means of small channels (plasmodesmata) and apoplastic, which is defined as movement of water into the cell wall and the intercellular free space [13, 14].

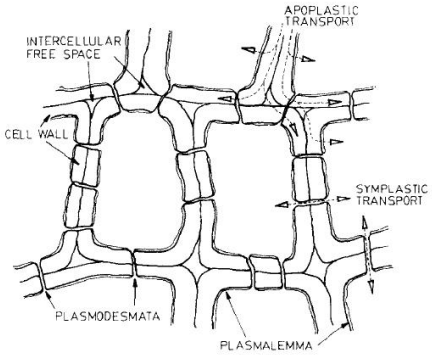

Figure 1: Mass transport pathways in the cellular structure of plant cells [13].

Most models of heat transfer on porous structures in food with interconnected pores assume the liquid water and water vapour phases remain in thermodynamic equilibrium at the local temperature [1, 2, 3, 4] but we note that [6] used two energy equations in the modelling of microwave heating: one for the liquid and solid phase and a second for the gas phase. [7] also used two energy equations, core and crust and the findings showed that the temperature between these two regions was different. In this study, a system of two energy equations, one equation for the intracellular cell and the other for the intercellular space, to describe the energy exchange in the tissue.

2.1 Free liquid water in intracellular cell (M_f)

A cell level model for the localised transport of water within the free water region is characterized by the following internal mechanisms: Transport of free liquid water through the cell walls and membranes into the intercellular space, transport of free liquid water from cell to cell and interchange of free liquid water from the bound state to the free state within individual cells, which is anticipated to be of smaller magnitude during active drying periods. The mechanisms are operational at the microscale and, for the current modelling, must be represented by appropriate models within the macroscale equations. Formulation of such macroscopic equations for water transport in porous media has been used in macroscopic model develop-

ment for the water transport relevant to the free water. A mass conservation equation for free water (M_f) is taken as

$$\rho_s \frac{\partial M_f}{\partial t} = \nabla.(D_f \rho_s \nabla M_f) + \nabla.(D_p \rho_s M_f \nabla P_c) - j_{ip} - j_{ic} + \rho_s r_b, \quad (1)$$

where D_f is effective diffusivity of free liquid water and D_p is effective diffusivity of plasmodesmata, ρ_s is density of solid phase. The first term on right hand side of equation (1) is the flux of water due to the differential gradient of free moisture level in the cells, the second is the flux of water due to differential gradient pressure in cells which is dependent on the local level of free water (M_f) and the gradient of cell pressure P_c, the third and fourth is sink term (change of liquid water to water vapour j_{ip} and j_{ip}) and fifth is a source term (from bound water).

Following [14] the release of free water from the intracellular cell into the intercellular space arises from differences between local pressure (j_{ip}) cumulatively occurs along the interconnected spaces. Thus, the mass flux of free water is associated with the differential pressure between the local cell and intercellular space and is taken as

$$j_{ip} = k_p(P_c - P_i). \quad (2)$$

In (2), k_p is a transfer coefficient and a measure of local cell pore permeability, number density and size, P_c and P_i is intracellular cell and intercellular space pressure respectively.

The local transport of free water from cell across the cell membranes to the intercellular space will be dependent on the differential moisture levels across the membrane. According to [13], transmembrane transport, defined as exchanges between the cell interior (cytoplasm and vacuole) and the cell exterior (cell wall and intercellular space) across the cell membrane, occurs in some instances. Correspondingly a macroscopic average of this cell transfer (j_{ic}) is taken to be in the form of a difference in volumetric densities, i.e.

$$j_{ic} = k_w(C_{fw} - C_i), \quad (3)$$

with C_{fw} as a concentration of free water in cell and C_i as a concentration of water in intercellular space.

The concentration of water in the intercellular space (C_i) is given by $C_i = \xi \rho_w$, where the density of intercellular space water vapour is given from the two-phase partition $\rho_i = \xi \rho_w + (1 - \xi)\rho_a$, where ξ is the level of liquid water within the intercellular space. This gives

$$C_i = \left(\frac{\rho_i - \rho_a}{\rho_w - \rho_a}\right)\rho_w, \quad (4)$$

with ρ_a, ρ_w, ρ_i is density of air, water, and intercellular water vapour respectively.

Concentration of water in the intracellular cell (free water region), in terms of free water moisture is given as

$$C_{fw} = \frac{M_f}{\frac{\rho_w}{\rho_s} + M_f}\rho_w. \quad (5)$$

2.2 Water vapour inside intercellular space (ρ_i)

Global models for transport of fluid (liquid and gas) through a porous food structure, for low Reynold number flow, have been well documented in terms of a Darcy Law [15]. Mass conservation for water vapour in the intercellular space is given by a general mass conservation equation [3] for a porous medium as

$$\frac{\partial(\phi_i \rho_i)}{\partial t} = \nabla.\boldsymbol{n}_i + j_{ip} + j_{ic}, \quad (6)$$

with $\boldsymbol{n}_i = \frac{k_i \rho_i}{\mu_i}\nabla P_i + D_i \nabla \rho_i$, where $\phi_i \rho_i$ is local mass flux of water vapour in the intercellular space, ρ_i is density of water vapour, where D_i is intercellular space diffusivity and k_i is the permeability of the food in the intercellular space. The first term on right-hand side of Eq. (6) is convective flow of water vapour within the intercellular space is anticipated as driven by an internal pressure gradient and resisted by viscous resistance from local viscous shear forces arising from the internal connective geometry, the second is diffusive flux of water vapour arises from any moisture gradient, and the third and the forth are source terms.

2.3 Bound water (M_b)

Within the cell structure, a small proportion of the water is identified as constrained by strong bonds to the cell structure and not freely available for transport by the more dominant diffusion mechanisms until free water content is relatively low. Following [16], bound water can be considered mobile only after conversion to the free water state. Initially, the portion of free moisture content is very large. The free moisture molecules diffuse through the bulk and evaporate at the boundary of the material. As drying continues, the bound moisture molecules are in the majority. Then the conversion between bound and free water controls the overall mass transfer phenomenon, leading to the decreased drying rate.

The interaction of bound water within the macroscopic multiphase model is taken as

$$\frac{\partial M_b}{\partial t} = -r_b = -(n_1 M_b - n_2 M_f). \quad (7)$$

In (7), M_b is the moisture level in the bound state and r_b is a corresponding conversion rate. n_1 and n_2 are kinetic constant define by Kiranoudis *et al.* [16], a model that depends on local moisture levels for free and bound water content is given by a weighted balance between the local levels of bound and free water. The difference between the two rates equals the decrease in bound water and the increase in free water inside the particle. This binding of water to the cell structure is responsible for the high residual water content, even after significant drying and is responsible for maintaining much of the structural integrity of the food in the later stages of drying. Correspondingly the level of air/shrinkage associated with the bound water region is anticipated to be negligible, other than in the final drying state.

2.4 Intercellular space temperature (T_i) and intracellular cell temperature (T_c)

In this study, the formulation of an energy balance included the possibility that two representative temperatures are relevant: a representative temperature of water vapour in the intercellular space T_i may differ from a representative temperature within the intracellular cell structureT_c. This will utilize the principle of local non-equilibrium between the cell and the intercellular space to formulate the energy exchange between the cell and intercellular space at a given location. This requires a system of two energy equations, one equation for the cell and the other for the intercellular space, to describe the energy exchange in the tissue.

A composite energy equation for the intercellular space is given by a conservation balance e.g. see [17], given by

$$\begin{aligned}\phi_i\rho_i c_i(\frac{\partial T_i}{\partial t}+\frac{\boldsymbol{n}_i}{\rho_i}\nabla T_i) &= \nabla.(\phi_i\kappa_v\nabla T_i)\\ &+ h_i A_{spec}(T_c-T_i)+(j_{ip}+j_{ic})c_i(T_c-T_i)\\ &- \lambda(j_{ip}+j_{ip}).\end{aligned} \tag{8}$$

where c_i is the heat content of water vapour and will be taken to be the same as the effective heat capacity of the cell c_{pw} and $\boldsymbol{n}_i$ is a mass flux (convective and diffusive fluxes) within intercellular space, h_i is an appropriate heat transfer coefficient which will involve a measure of the interface area A_{spec} associated with the porous structure, κ_v is effective conductivity and λ is the latent heat. The first term on right-hand side of Eq. (8) is conductive flow of heat, the second term is inflow of heat is due to the difference between the temperatures in the intercellular space and the intracellular tissue structure, the third term is heat is transported from the intracellular cell into the intercellular space due to water release from the cell wall pores and cell membrane, the forth term is evaporation from water to water vapour requires an amount of heat for the phase transition.

Within the cellular tissues, the predominant heat transfer mechanism within the cells will arise from local conduction within the intracellular cell phase and heat transfer within the intercellular space phase. A common temperature associated with the intracellular cell phase is taken as T_c, arising from the relatively high conductivity of water and solid tissues. The heat capacity of any air within the cell structure is taken as negligible. A corresponding form for the energy equation for the intracellular cell phase, (see [17, 15]), is given by

$$\begin{aligned}(1-\phi_i)\rho_c c_{pw}\frac{\partial T_c}{\partial t} &= (1-\phi_i)\nabla.(\kappa_c\nabla T_c)\\ &- h_i A_{spec}(T_c-T_i)-(j_{ip}+j_{ic})c_{pw}(T_c-T_i),\end{aligned} \tag{9}$$

where c_{pw} is the effective heat capacity of the cell structure and κ_c is the effective conductivity.

3 Equation of state and phenomenological relations

To supplement the simultaneous heat and mass equations, closure of the system requires an equation of state or phenomenological physical relationships for the exchange processes between the intracellular cell and intercellular space.

3.1 Intercellular space pressure (P_i)

Water vapour released within the intercellular space is of sufficiency low density such that the water vapour is governed by the perfect gas law, hence

$$P_i = \rho_i R T_i. \tag{10}$$

Substituting non-dimensional parameter in the perfect gas law gives

$$\overline{P}_i = \overline{\rho}[1+\frac{(T_a-T_0)}{T_0}\overline{T}_i]. \tag{11}$$

3.2 Phase change

In most drying and frying processes, evaporation distributed inside the food domain exists, such as discuss by [18] and [11]. This suggests that the measure of vapour pressure and water activity may not be appropriate in modelling of fast transport processes of

water vapour due to the time taken to reach equilibrium. [18] discuss the evaporation rate using a non-equilibrium approach that has been used in porous media models . In our modelling, this formulation is appears in equations (1),(6),(8) and (9) and is related to the current formulation by

$$\dot{I} = j_{ip} + j_{ic}. \tag{12}$$

3.3 Intracellular cell pressure (P_c)

The difference in pressure is evaluated in relation to the change of cellular volume through a measure of the reversible elastic properties of the cell walls in the form of an empirical modulus ς [14] and following [19], due to water lost from the cells because of drying leads to

$$dP_c = \varsigma \frac{dM_f}{M_f}, \tag{13}$$

where P_c is the osmotic pressure in the cellular cell above atmospheric pressure. As discussed by [19], it is assumed that ς is not a function of P_c. Hence, integrating equation (13) yields

$$P_c = \varsigma\, ln\, \frac{M_f}{M_{f0}} + P_{c0}. \tag{14}$$

The value of ς given by [20], stated at the incipient plasmolysis point where the turgor pressure is equal to the environment pressure, is given by 3.5. The value of P_{c0} will given as turgor pressure at the beginning, as discussed in the case of constant internal pressure as 159kPa.

4 Initial and boundary conditions

Five second order of differential equations have been derived to describe the heat and mass transfer in the intercellular space and the intracellular cell. Initially, the food material is at ambient pressure and temperature conditions, given by $P_i(t = 0) = P_{atm}$, $T_i(t = 0) = T_{i0}$ and $T_c(t = 0) = T_{c0}$.

Depending on the composition of food material, the initial phase of the free water, bound water and water vapour is estimated. Initially, intercellular space contains air and gives by $\rho_i(t = 0) = \rho_a$. Free water and bound water initial conditions are given by, $M_f(t = 0) = M_{f0}$ and $M_b(t = 0) = M_{b0}$.

Boundary conditions on the closed boundary at x=0 for intercellular space and intracellular cell, assuming symmetry condition, the mass and heat flux are given below,

$\mathbf{n}.(\nabla T_i) = 0$, $\mathbf{n}.(\nabla T_c) = 0$, $\mathbf{n}.(\nabla M_f) = 0$, $\mathbf{n}.(\nabla M_b) = 0$, and $\mathbf{n}.(\nabla \rho_i) = 0$.

At the surface, there is an exchange of heat, liquid water, vapour with surrounding air. Moisture is transported to the surrounding air from the food surface in either liquid or vapour form, depending upon the intensity of drying. Following [5], the boundary conditions for intercellular space at the surface are obtained from flux balances and given by

$$-h_{m,v}(\rho_{i,sur} - C_{air}) = \frac{k_i \rho_i}{\mu_i} \nabla P_i + D_i \nabla \rho_i, \tag{15}$$

In the intracellular cell, the boundary conditions applied to the external surface of food express the balance between the diffusive flux of liquid water coming from the core of the food and the flux of vapour leaving the food surface that is transferred to the drying air is given by

$$-h_{m,f}(C_{fw,sur} - C_{air}) = D_f \rho_s \nabla M_f + H_p M_f \rho_s \nabla P_c. \tag{16}$$

The quantities $h_{m,v}$ and $h_{m,f}$ are associated with the mass transfer coefficient of vapour and the free water phase,μ_i is viscosity. $\overline{C}_{fw,sur}$ such as given by the relationship between water vapour pressure and concentrations of water vapour at the surface, which link the surface concentration C_{sur} and surface temperature T_{sur} (see [21]). An energy balance over the interface, the heat flux arriving at the surface from the interior of the materials equals the heat flux leaving the interface by convection. In the intercellular space, the boundary condition becomes

$$-\phi_i h_i (T_{isur} - T_{air}) = \phi_i \kappa_v \nabla T_i. \tag{17}$$

If liquid water is transferred from the food surface to the processing air, heat is needed to evaporate the water at the product surface. It is supplied by processing air so that the intracellular cell boundary condition becomes

$$\begin{aligned} -(1-\phi_i) h_c (T_{csur} - T_{air}) &= (1-\phi_i)\kappa_c \nabla T_c \\ &- \lambda \Big(D_f \rho_s \nabla M_f + H_p M_f \rho_s \nabla P_c \Big). \end{aligned} \tag{18}$$

The quantities h_i and h_c are associated with the heat transfer coefficient of the intercellular space and the intracellular cell.

5 Non-dimensional formulation

The system of equations that governs the drying process is given in equations (1),6), (7), (8) and equation (9). To simplify the equations, the following scaling groups are used, where the overbar correspond to a non-dimensional variable,

$$\overline{x} = \frac{x}{L_0}, \quad \tau = \frac{D_0 t}{L_0^2},$$

$$\overline{\rho} = \frac{\rho_i}{\rho_a}, \quad \overline{P}_i = \frac{P_i}{P_{atm}}, \quad \overline{P}_c = \frac{P_c}{P_{atm}},$$
$$\overline{\rho}_c = \frac{\rho_c}{\rho_a}, \quad \overline{\rho}_s = \frac{\rho_s}{\rho_a} \quad \overline{k} = \frac{k_i P_{atm}}{\mu D_0},$$
$$\overline{D}_i = \frac{D_i}{D_0}, \quad \overline{D}_f = \frac{D_f}{D_0} \quad \overline{D}_p = \frac{D_p P_a}{D_0},$$
$$\overline{T}_i = \frac{T_i - T_0}{T_{air} - T_0}, \quad \overline{T}_c = \frac{T_c - T_0}{T_{air} - T_0}.$$

In the above L_0 is taken as characteristic dimension of the food and D_0 a suitable diffusion coefficient scaling. Other source or sink terms associated with the formulation are

$$\overline{j}_{ip} = \frac{L_0^2}{D_0 \rho_a} j_{ip}, \quad \overline{j}_{ic} = \frac{L_0^2}{D_0 \rho_a} j_{ic},$$
$$\overline{n}_1 = n_1 \frac{L_0^2}{D_0}, \quad \overline{n}_2 = n_2 \frac{L_0^2}{D_0},$$

Substituting these dimensional quantities into all the equation and assuming that the sample undergoes one dimensional movement parallel to the x-axis and interacting with the temperature between phases, and a summary of mathematical model developed is given below:

$$\phi_i \frac{\partial \overline{\rho}}{\partial \tau} = \frac{\partial}{\partial x}\left[(\overline{\rho}\overline{k}\gamma + \overline{D}_i)\frac{\partial \overline{\rho}}{\partial \overline{x}}\right] + \overline{j}_{ip} + \overline{j}_{ic} \quad (19)$$

$$\phi_i \overline{\rho}\left[\frac{\partial \overline{T}_i}{\partial \tau} + \frac{\boldsymbol{n}_i}{\overline{\rho}}\frac{\partial \overline{T}_i}{\partial \overline{x}}\right] = \frac{\partial}{\partial \overline{x}}\left[\phi_i \overline{\kappa}_v \frac{\partial \overline{T}_i}{\partial \overline{x}}\right] + \overline{h}_i(\overline{T}_c - \overline{T}_i) + (\overline{j}_{ip} + \overline{j}_{ic})(\overline{T}_c - \overline{T}_i) - \lambda(\overline{j}_{ip} + \overline{j}_{ic}) \quad (20)$$

$$\overline{\rho}_s \frac{\partial M_f}{\partial \tau} = \frac{\partial}{\partial \overline{x}}\left[\overline{D}_f \overline{\rho}_s \frac{\partial M_f}{\partial \overline{x}} + \overline{D}_p M_f \overline{\rho}_s \frac{\partial \overline{P}_c}{\partial \overline{x}}\right] - \overline{j}_{ip} - \overline{j}_{ic} + \overline{r}_b \overline{\rho}_s \quad (21)$$

$$\frac{\partial M_b}{\partial \tau} = \overline{n_1} M_b - \overline{n_2} M_f \quad (22)$$

$$(1-\phi_i)\overline{\rho}_c \frac{\partial \overline{T}_c}{\partial \tau} = \frac{\partial}{\partial \overline{x}}\left[(1-\phi_i)\overline{\kappa}_c \frac{\partial \overline{T}_c}{\partial \overline{x}}\right] - \overline{h}_i(\overline{T}_c - \overline{T}_i) - (\overline{j}_{ip} + \overline{j}_{ic})(\overline{T}_c - \overline{T}_i) \quad (23)$$

$$\overline{j}_{ip} = \overline{k}_p(\overline{P}_c - \overline{P}_i) \quad (24)$$

$$\overline{j}_{ic} = \overline{k}_w(\eta - \xi) \quad (25)$$

Initial Conditions:

$$M_f = 3.7, M_b = 0.39, \overline{\rho} = 1, \overline{T}_i = 0, \overline{T}_c = 0 \quad (26)$$

Boundary conditions on the closed boundary at $\overline{x} = 0$, assuming symmetry boundary,

$$\frac{\partial M_f}{\partial \overline{x}} = 0, \frac{\partial M_b}{\partial \overline{x}} = 0, \frac{\partial \overline{\rho}}{\partial \overline{x}} = 0, \frac{\partial \overline{T}_i}{\partial \overline{x}} = 0, \frac{\partial \overline{T}_c}{\partial \overline{x}} = 0, \quad (27)$$

Non-dimension mass transfer boundary conditions at the surface for free water and intercellular space, at $\overline{x} = 1$, are given by

$$\left[\overline{D}_f \overline{\rho}_s \frac{\partial M_f}{\partial \overline{x}} + \overline{D}_p M_f \overline{\rho}_s \frac{\partial \overline{P}_c}{\partial \overline{x}}\right] = -Sh_f(\overline{C}_{fw,sur} - 1) \quad (28)$$

$$\left[(\overline{\rho}\overline{k}\gamma + \overline{D}_i)\right]\frac{\partial \overline{\rho}}{\partial \overline{x}} = -Sh_i\left(\frac{\overline{\rho}}{\overline{C}_{air}} - 1\right) \quad (29)$$

Non-dimension energy balance at the surface for intercellular space and intercellular cell boundary, at $\overline{x} = 1$ are given by

$$-\phi_i Nu_i \overline{\kappa}_v(\overline{T}_{isur} - 1) = \phi_i \overline{\kappa}_v \frac{\partial \overline{T}_i}{\partial \overline{x}} \quad (30)$$

$$-(1-\phi_i)\overline{\kappa}_c Nu_c(\overline{T}_{csur} - 1) = (1-\phi_i)\overline{\kappa}_c \frac{\partial \overline{T}_c}{\partial \overline{x}} - \overline{\lambda}\left[\overline{D}_f \overline{\rho}_s \frac{\partial M_f}{\partial \overline{x}} + \overline{D}_p M_f \overline{\rho}_s \frac{\partial \overline{P}_c}{\partial \overline{x}}\right] \quad (31)$$

with $\overline{C}_{fw,sur} = f(M_f)\beta(\overline{T}_i)$ as discuss in [22].

Non-dimensional parameters are

$$Sh_f = \frac{h_{m,f} L_0}{D_0}\frac{C_{air}}{\rho_a}, Sh_i = \frac{h_{m,v} L_0}{D_0}\frac{C_{air}}{\rho_a},$$
$$\overline{\kappa}_v = \frac{\kappa_v}{D_0 c_{pw} \rho_a}, \overline{\kappa}_c = \frac{\kappa_c}{D_0 c_{pw} \rho_a}, \overline{k}_p = \frac{k_p P_a L_0^2}{D_0 \rho_a},$$
$$\overline{k}_w = \frac{k_w L_0^2 \rho_w}{D_0 \rho_a}, Nu_i = \frac{\overline{h}_i L_0}{\kappa_v}, Nu_c = \frac{h_c L_0}{\overline{\kappa}_c},$$
$$\overline{h}_i = \frac{h_i L_0^2 A_{spec}}{c_{pw} D_0 \rho_a}, \overline{r}_b = \frac{r_b L_0^2}{D_0}, \overline{\lambda} = \frac{\lambda}{c_{pw}(T_a - T_0)},$$
$$\eta = \frac{M_f}{\frac{\rho_w}{\rho_s} + M_f} \text{ and } \xi = \frac{\overline{\rho} - 1}{\frac{\rho_w}{\rho_a} - 1}.$$

6 Numerical solution

A one-dimensional model is employed in the analysis since the sample approximates an infinite slab of thickness $2L$ with one end insulated and influx boundary at the surface. Numerical solutions were sought for the five dependent variables $\overline{\rho}$, M_f, M_b, $\overline{T}_i$ and $\overline{T}_c$.

Table 1: Equation generates for intercellular space region.

Coefficient	Value Expression
e_a	0
d_a	ϕ_i
Γ(flux vector)	$-(\rho\, k\gamma + D_i)\frac{\partial \rho}{\partial x}$
F(source term)	$j_{ip} + j_{ic}$

These equations were solved using COMSOL Multiphysics. COMSOL is a PDE-based multiphysics tool that makes use of finite element modeling (FEM). A mesh consisting of 2400 quadrilateral elements was constructed and the equation for moisture and temperature was solved using UMFPACK solver. In the general equation system forms, the PDEs and boundary conditions are written in the following form:

$$\begin{cases} e_a \dfrac{\partial^2 u}{\partial t^2} + d_a \dfrac{\partial u}{\partial t} + \nabla.\Gamma = F & \text{in } \Omega, \\ -\mathbf{n}.\Gamma = G - h^T \mu & \text{on } \partial\Omega, \\ 0 = R & \text{on } \partial\Omega. \end{cases}$$

For example equation (19) were input into COMSOL Multiphysics using the a partial differential equation (PDE) solver with the general equation system form.

$$\phi_i \frac{\partial \rho}{\partial \tau} + \frac{\partial}{\partial x}\Big[-(\rho\, k\gamma + D_i)\frac{\partial \rho}{\partial x}\Big] = j_{ip} + j_{ic},$$

Identifying the general form, the following settings generate the equation in Table 1

The time dependent problem was solved by an implicit time-stepping scheme, leading to non linear system of equations for each time step. Newton's method was used to solve each non-linear system of equations, whereas a direct linear system solver was adopted to solve the resulting systems of linear equations. The relative and absolute tolerance were set to 10^{-4} and 10^{-5}, respectively. The drying process is considered to be completed when the moisture content in the sample is asymptotic to a residual level.

We remark here that, due to the absence of experimental data on which to base our model parameter values and the fast timescale chosen, in all subsequent numerical simulations, the parameter values are selected from the literature data to illustrate the behaviour of the model under a particular movement regime. In the first instance, a range of non-dimensional physical relevant values are shown in Table 2.

7 Results and discussions

Solution of the model is obtained from solving five coupled PDEs, corresponding to mass and temperature equations (eq 19-23), together with equations of transfer flux (eq 24-25), with initial and boundary conditions (eq 26-31). For the first simulation, simplification is taken that the value of internal turgor pressure $\overline{P}_c$ remains constant and above atmospheric pressure P_{atm} during the main drying stage as $\overline{P}_c$=1.59. This will give the term $\overline{D}_p\, M_f\, \overline{\rho}_s \dfrac{\partial \overline{P}_c}{\partial \overline{x}} = 0$ in equation (21), (28) and (31). The effect of bound water (eq 22) where not included in this analysis (two phase model).

Table 2: Non-dimension parameter values.

Non-dimensional parameter	Value	Range of value.
Sh_i	5	1-20
Sh_f	20	0.1-20
$\overline{D}_f$	1	0-2
$\overline{D}_i$	1	1-10^4
$\overline{k}$	1	1-10^4
$\overline{k}_p$	10^{-2}	0-1
$\overline{k}_w$	10^{-2}	0-1
Nu_i	5	0-20
Nu_c	5	0-20
$\overline{\kappa}_v$	5	0.1-100
$\overline{\kappa}_c$	5	0.1-100
$\overline{\lambda}$	0.5	0-1

Figure 2 and 3 shows the typical trends of the cell and intercellular space temperature, free water moisture and intercellular vapour density at the surface and center of the fruit during drying. From the cell temperature profile (figure 2(b)), three different stages can be defined: the initial steep temperature rise is the result of heat transfer, dependent on convection due to temperature difference between air and food (normalize time τ=0-0.3); the temperature increases to a new constant and remains stationary while latent heat prevents a temperature rise (normalize time τ=0.3-1.8) and then there is a further rise to its maximum steady state temperature (normalize time τ=1.8-3). A similar result for the drying of mango is reported by Tour and Kibangu-Nkembo [24], who studied the solar drying of mangos in a hurdle-dryer with a wire net bottom, observing that, during the constant rate period, the product temperature was lower than the ambient air temperature with an average difference of 2.3^{o}C and remaining at a constant temperature until a certain value of moisture.

Figure 2(a) shows that, initially, when the process is controlled by external heat transfer and water leaving the surface was not bound to the food structure,

the moisture loss attained a maximum value (normalize time τ=0-0.3). Afterwards, when the process was controlled by mass transfer and the water leaving the surface was bound to the food structure, a progressive decrease in the drying curve was observed (normalize time τ=0.3-1.8). As the free water moisture became very low at normalize time $\tau = 2$, the latent heat $\overline{\lambda}$ at the boundary condition at the surface (eq 31) was no longer effective and this led to a final decrease in moisture and a final increase in temperature at the end of drying. With respect to most work published in the literature, this typical trend of free water moisture shown in our simulations was observed in experimental drying, such as the drying of carrot [25], banana [26] and cucumber [23].

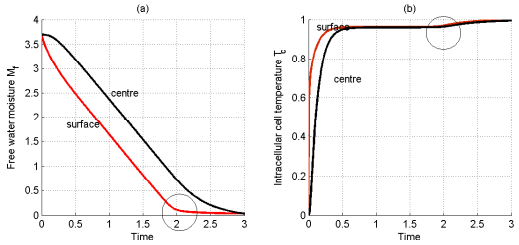

Figure 2: Profile of (a) free water moisture M_f (b) cell temperature $\overline{T}_c$ at the surface and the center. Dimensionless parameter values given by $Sh_f = 20$, Sh_i=5, $\overline{D}_f$=1, $\overline{D}_i$=1 $\overline{k}$=1, $\overline{k}_p$=0.01, and $\overline{k}_w$=0.01, Nu_i=5, Nu_c=5, $\overline{\kappa}_c$= 5, $\overline{\kappa}_v$= 5 $\overline{\lambda} = 0.5$.

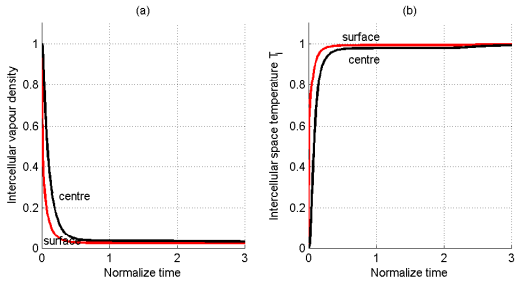

Figure 3: Profile of (a) intercellular vapour density $\overline{\rho}$ (b) intercellular temperature $\overline{T}_i$ at the surface and the centreline. Parameter values as in figure 2

Figure 3(b) shows that the temperature profile in the intercellular space increases rapidly during early heating; the source of heat from air drying is very effective at the beginning. As heating progresses, the rise in temperature attains an almost uniform profile indicating that the process has basically approached a steady state. The temperature is higher at the surface and intercellular vapour density decreases much faster at the surface. Figure 3(a) shows intercellular vapour density decreasing with time. The sources of vapour inside the intercellular space are from the transfer fluxes. As a result of water advected to the pores (intercellular space), the water inside the intercellular space increases. Then the thermal process occurs, which induces strong water evaporation in this area. As a result, more vapour is produced inside the pores. Intercellular vapour density decreases due to the flow of vapour from the surface due to permeability and diffusive flow. Some studies (for example see [27]) have stated that a decrease in the local density of vapour causes the water to evaporate at a lower temperature, depend on permeability to gas flow and water vapour diffusion.

Comparing figure 2(a) with figure 3(a), the time taken for free water to reach equilibrium at the surface is $\tau = 2$ but, for vapour, the time taken is $\tau = 0.4$, and consistent with other study [27] that shows the rate of water vapour transfer to the sample surface to be much faster than the free water transport to the drying front by several orders of magnitude. Comparing figure 2(b) with figure 3(b), intercellular space temperature $\overline{T}_i$ rises more rapidly compared to intercellular cell temperature $\overline{T}_c$. By inspection equation (20), heat was used for internal evaporation inside the intercellular space for water evaporation but the source of heat for the intercellular space comes from convection from overlying air and transfer fluxes from the cell. This leads to a higher increase in temperature inside intercellular space. Similar conclusions have been drawn by other study: for instance, Farkas *et al.* [7] have shown temperature is higher inside the crust region, which is characterized by vapour flow, compared to the core region, which is dominated by the liquid phase.

Figure 4 shows how the centreline free water moisture and intercellular vapour density, representative cell temperature and intercellular space temperature profile are created by the modifying effect of pressure. The modifying effect of pressure inside the cell through pressure dependent on the volume of water loss was put back into the model equation (eq 21) and through the boundary condition(eq 28 and 31). The effect of bound water is not included in the analysis. As in the two-fluid model, under constant pressure, free water flow will be driven by pressure to the intercellular phase, but there is no pressure driven from the deeper cell through plasmodesmata and so $\overline{D}_p\, M_f\, \overline{\rho}_s \dfrac{\partial \overline{P}_c}{\partial \overline{x}} = 0$. This leads to a slower decrease of free water M_f (figure (a)). High pressure water driven into the intercellular space, brings heat with it, leading to a slow increase in cell temperature $\overline{T}_c$ (figure (c)). The intercellular vapour density will decrease more

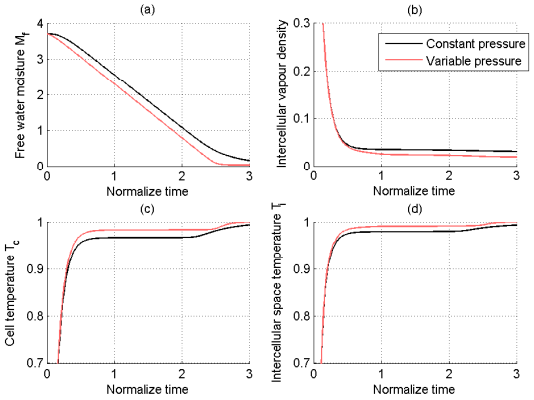

Figure 4: Profile of intercellular space temperature, vapour density, intracellular cell temperature and free water moisture at the centreline. Dimensionless parameter values given by $Sh_f = 20$, Sh_i=5, $\overline{D}_f$=1, $\overline{D}_i$=1 $\overline{k}$=1, $\overline{k}_w$=0.01, $\overline{k}_p$=0.01, Nu_i=5, Nu_c=5, $\overline{\kappa}_c$= 5, $\overline{\kappa}_v$= 5 and $\overline{\lambda} = 0.5$

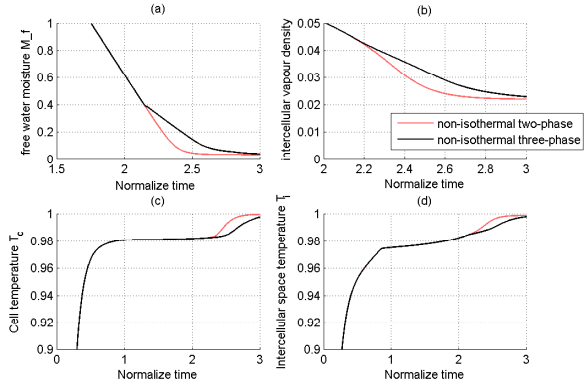

Figure 5: Profile of free water moisture, intercellular vapour density, cell temperature and intercellular temperature for two-phase and three-phase non-isothermal case at the surface. Parameter values the same as Figure 4

slowly due to higher pressure driven water to flow from the cell structure (figure (b)). With increased water in the intercellular space, more heat is needed for water evaporation, leading to a lower intercellular space temperature (figure (d)). For variable pressure, there is a convective flow because pressure is driven from deeper cells to the surface, in addition to transfer flux because of pressure driven flow into intercellular space. These two flows will give faster transfer of free water compared to constant pressure (figure (a)). Due to the balance between pressure mechanisms, the flow will be distributed within transfer flux to the intercellular space and convective driven flow to the external surface, so that the intercellular vapour density produced will be lower (figure (b)). This leads to a higher intercellular space temperature $\overline{T}_i$ because less heat is needed for evaporation (figure (d)). At the same time, because of the balance between pressure mechanisms, cell temperature $\overline{T}_c$ will also be higher in the case of variable pressure.

Comparison of the two-phase and the three-phase models (the effect of bound water is included) are shown in figure 5. Figure 5 shows a profile of free water moisture, intercellular vapour density, cell temperature and intercellular space temperature for two-phase and three-phase non isothermal cases at the center. Comparison of the two-phase and the three-phase models shows the decrease in free water as nearly the same, but at a later stage in the three-phase model, the transfer of bound water to free water increases the level of free water moisture in cell (refer Figure 5(a)) leads to increasing transfer flux into intercellular space. This happens in the later stage (normalize time $\tau = 2.3$) when $M_f < M_b$. This gives the intercellular vapour density to be higher at the end of drying. Figures 5(c) and 5(d) show a profile of temperature at the surface of the intercellular space and the intracellular cell. The temperature of three-phase model is little bit lower at τ=2.3, which happens as the transfer of bound water to free water leads to increased of free water moisture levels. This water is advected to the intercellular space, particularly increasing the intercellular vapour density. This gives the increase in cell temperature $\overline{T}_c$ and intercellular space temperature $\overline{T}_i$ at a later stage in the three-phase model, which is slower than the two-phase model.

8 Comparison with literature data

There is only limited experimental transport data for cellular tissues available in the literature. Most data are expressed as diffusion coefficients and are obtained from solution of the diffusion coefficient along with the experiment drying curve on the basis of physical models unlike those presented in this work. Alternatively, prediction used in the theoretical model result can be compared on the basis of some assumptions in the literature data. Comparison was made with the work of [28], who investigated the convective drying of mango with the effects of shrinkage and that of [29] for apple drying. Figure 6 shows the variation in moisture content by drying time for air velocity=0.8 m/s, RH=15%, temperature=70^{o}C and length=5mm for mango drying and velocity=1 m/s, temperature=60^{o}C, RH=9%, length=5mm for apple

drying. As seen, the comparison between experiment results of moisture and model prediction matches closely with the results of [28] and [29]. At the beginning, there is close agreement between experiment data simulation at high moisture content; at low moisture contents, the predicted value begins to separate from experiment data. This departure is to be expected because the model is built on the assumption that cellular structure remains functional. This is less and less realistic as moisture content decreases, because of an increasing portion of tissue becoming non functional. This similar behaviour was also observed by [12] when they compared experiment data with their simulation. As our model considers vapour transport to be distributed across the cell structure at the later stage of drying; this transport leads to a faster decrease at the end of drying compared to their model. Such close agreement between experiment measurements and model prediction confirms the effectiveness of the model and serves to validate it.

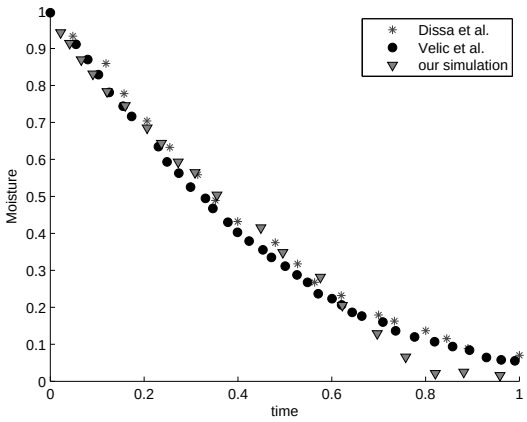

Figure 6: Comparison between numerical solutions for moisture with experiment data from the literature by [28] and [29]. Dimensionless parameter values the same as figure 1

9 Conclusions

In this paper, we have developed a multi-phase model for the movement of water and heat during drying of tropical fruits by developing a representative model that is based on their cellular structure. Based on this cellular features at cell level, the model was derived using multiphase approach; each material constituent is taken as a distinct phase within the multiphase and with the constitutive law describing the material properties and its interaction with the neighboring phase. To include interaction between neighboring phases, we incorporate source terms j_{ip} and j_{ic} into the appropriate mass balance equations. Transfer fluxes j_{ip} and j_{ic} relates moisture transfer from intracellular cell into intercellular space lies at the heart of this new drying model. In case of equation of state was considered [30] suggest that logarithmic-correction exponent can enhance the decay to zero in which such correction can be considered in moisture and vapour situation in this modelling.

Simulations of the model were based on non-isothermal conditions for a two-phase model. Model simulation results show the behaviour changes in liquid water and water vapour during drying. Model simulations yielded behaviour of liquid water transport similar to that seen in the single phase model. The multi-phase model also generates results not evident in the homogenous model, such as the behavior of water vapour inside the intercellular space. The modifying effect of including bound water within the cellular structure is provided within a three-phase model. Simulations were presented, showing that the flow of moisture in the intracellular cell is profoundly altered by this effect, especially in the later stage of drying. This simulation demonstrates the importance of considering the effect of bound water within drying to low levels of moisture retention. We conclude that with the adding of bound water in the model gives influence in drying especially at the later stage of drying to reduce residual level of moisture.

The effect of internal cell pressure was included in the model through constant pressure and pressure decreases due to lost of moisture. To include the transport of water from one cell to another cell through cell walls pores (plasmodesmata), variable pressure was put into the models. For this case, free water will be driven from deeper cells to the surface, by differential gradient of internal pressure. Simulations were presented showing that the flow of water in intracellular cell is faster for variable pressure compared to constant pressure.

The additional effect of heat considers the principal of local non-equilibrium between the cell and intercellular space at given locations. This given by representative temperature in the intercellular space $\overline{T}_i$ which is different from representative temperature within the intracellular cell $\overline{T}_c$. This could not be seen in the single phase model, which assumed heat transfer remains in equilibrium at the local temperature. Our model reveals that temperature gives significant effects in both intercellular space and intracellular cells. This prediction has important implications for food engineering applications, suggesting that a uniform temperature is crucial, as temperature is the main source of drying.

Acknowledgements: The authors wish to thank the Government of Malaysia, Universiti Teknologi MARA Malaysia, and The University of Nottingham, UK. Thanks are due to Dr. S. Hill, Dr N. Alias and Dr P. Gajjar for their suggestions and helpful discussions.

References:

[1] R. Yamsaengsung, and R. G. Moreira, Modeling the transport phenomena and structural changes during deep fat frying Part I: Model developement, *Journal of Food Engineering*, 53, 2002 pp. 1–10.

[2] H. Feng, and J. Tang, and R.P. Cavalieri, and O.A. Plumb, Heat and mass Transport in microwave drying of porous materials in a spouted bed, *AIChE Journal*, 47, 2001 pp. 1499–1512.

[3] H. Ni, and A.K. Datta, Moisture transport in intensive microwave heating of biometerial: a multiphase porous media approach, *International Journal of Heat and Mass Transfer*, 42, 1999, pp. 1501–1512.

[4] H. Ni, and A.K. Datta, Infrared and hot-air-assisted microwave heating of foods for control of surface moisture, *Journal of Food Engineering*, 51, 2002, pp. 355–364.

[5] A. Ousegui,and C. Moresoli, and M. Dostie, and B. Marcos, A Porous multiphase approach for baking process-Explicit formulation of evaporation rate, *Journal of Food Engineering*, 100, 2010, pp. 535–554.

[6] D. D. Dincov, and K A. Parrott, and K A. Pericleous, Heat and mass transfer in two phase porous materials under intensive microwave heating, *Journal of Food Engineering*, 65, 2004, pp. 403–412.

[7] B. E. Farkas, and R. P. Singh, and T. R. Rumsey, Modeling Heat and Mass Transfer in Immersion Frying. I, Model Development, *Journal of Food Engineering*, 29, 1996, pp. 211–226.

[8] H. Ni, and A K. Datta, Moisture, oil and energy transport during deep fat frying of food materials, *Trans IChem*, 77, 1999, pp. 194–204.

[9] A. Halder, and A K. Datta and R M. Spanswick, Water transport in cellular tissues during thermal processing, *Trans IChemE. Food and Bioproducts Processing* , 00, 2010, pp. 1–15.

[10] G. Fang, and C.A. Ward, Examination of the statistical rate theory expression for liquid evaporation rates: statistical physics, plasma fluids and related interdisciplinary topics, *Physics Review*, 59, 1999, pp. 441–453.

[11] A. Halder, and A. Dhall, and A.K. Datta, Modeling Transport in porous media with phase change: Application to food processing, *Journal of Heat Transfer*, 133, 2011, pp. 1–13.

[12] G. H. Crapiste, and S. Whitaker, and E. Rotstein, Drying of cellular structure-I. A mass transfer theory, *Chemical Engineering Science*, 43, 1988, pp. 2919–2928.

[13] C. J. Toupin,and M. Marcotte, and M. L. Maguer, and C. J. Michkle, Osmotically-Induced Mass Transfer in Plant Storage Tissues: A Mathematical Model. Part I, *Journal of Food Engineering*, 10, 1989, pp. 13–38.

[14] P. S. Nobel, *Biophysical Plant Physiology and Ecology* , W.H. Freeman and Co.,1983.

[15] A. K. Datta, Porous media approaches to studying simultaneous heat and mass transfer in food processes I:Problem formulation, *Journal of Food Engineering*, 80, 2007, pp. 80–95.

[16] C T. Kiranoudis, and Z.B. Maroulis, and D.A. Marinos-Kouris, Heat and Mass transfer model building in drying with multiresponse data, *Int J. Heat and Mass Transfer* , 38, 1995, pp. 463–480.

[17] R. B. Bird, and W. E. Stewart, and E. N. Lightfoot, *Transport phenomena*, John Wiley and son, 2002.

[18] J. Zhang, and A. K. Datta, Some consideration in modelling of moisture transport in heating of hygroscopic materials, *Drying Technology*, 22, 2004, pp. 1983–2008.

[19] J. Dianty, Water relations of plant cells, Edited: U. Luttge and M. G. Pitman, *Transport in plants II. Part A.F,* New York, USA: Academic Press, Springer-Verlag Springer, 1976.

[20] Y. Zhiming, and M. Le Maguer, Mathematical Modelling and Simulation of Mass Tansfer in Osmotic Dehydration Processes. Part II: Simulation and verification, *Journal of Food Engineering*, 32, 1997, pp. 21–32.

[21] N. Shahari, and S. Hibberd, Mathematical Modelling of shrinkage effect during drying of food, *CHUSER 2012 - 2012 IEEE Colloquium on Humanities, Science and Engineering Research*, 2012, pp. 249–254.

[22] Shahari, N. and Hibberd, S., Analysis of Single Phase Moisture and Heat Model of Food Drying *4th International Conference of Mathematical Models in Engineering and Computer Science*, 2013, pp. 127–142.

[23] Shahari, N. and Hussein, S.M. and Nursabrina, M. and Hibberd, S., Mathematical modelling of cucumber (cucumis sativus) drying, *AIP Conference Proceedings*, 2014, pp.307-312.

[24] S. Touré, and S. Kibangu–Nkembo, Comparative study of natural solar drying of cassava, banana and mango, *Renewable Energy*, 29, 2004, pp. 975–990.

[25] M. Aversa, and S. Curcio, and V. Calabro, and G. Iorio, An analysis of the transport phenomena occuring during food drying process, *Journal of Food Engineering*, 78, 2007, pp. 922–932.

[26] M E. Katekawa, and M. Silva, On the influence of glass transition on shrinkage in convective drying of fruits: a case study of banana drying , *Drying Technology*, 25, 2007, pp. 1659–1666.

[27] C. Di Blasi, Multi-phase moisture transfer in high-temperature drying of wood particles, *Chemical Engineering Sciences*, 53, 1997,pp. 353–366.

[28] A.O. Dissa, and H. Desmorieux, and J. Bathiebo, and J. Koulidiati, Convective drying characteristics of Amelie mango(Mangifera Indica L. cv. Amelie) with correction for shrinkage, *Journal of Food Engineering* , 88, 2008, pp. 429–437.

[29] D. Velič, and M. Planinič, and S. Tomas, and S. Bilič, Influance of air velocity on kinetics of convection of apple drying, *Journal of Food Engineering* ,64, 2004, pp. 97–102.

[30] M. Krasnytska, and B. Berche, and U. Holovatch., Phase transitions in the Potts model on complex networks, *Condensed Matter Physics*, 16, 2013 pp. 115